One-way transport in laser-illuminated bilayer graphene: A Floquet isolator

V. Dal Lago,[1,*] E. Suárez Morell,[2] and L. E. F. Foa Torres[3,†]

[1]*Instituto de Física Enrique Gaviola (CONICET) and FaMAF, Universidad Nacional de Córdoba, Córdoba, Argentina*

[2]*Departamento de Física, Universidad Técnica Federico Santa María, Valparaíso, Chile*

[3]*Departamento de Física, Facultad de Ciencias Físicas y Matemáticas, Universidad de Chile, Santiago, Chile*

(Received 9 August 2017; revised manuscript received 8 November 2017; published 8 December 2017)

We explore the Floquet band structure and electronic transport in laser-illuminated bilayer graphene ribbons. By using a bias voltage perpendicular to the graphene bilayer we show how to get one-way charge and valley transport among two unbiased leads. In contrast to quantum pumping, our proposal uses a different mechanism based on generating a nonreciprocal band structure with a built-in directionality. The Floquet states at one edge of a graphene layer become hybridized with the continuum on the other layer, so the resulting band structure allows for one-way transport as in an *isolator*. Our proof of concept may serve as a building block for devices exploiting one-way states.

DOI: 10.1103/PhysRevB.96.235409

I. INTRODUCTION

The advent of graphene [1–4] as well as the new family of two-dimensional (2D) materials and their heterostructures [5] has provided us with an outstanding playground for testing quantum transport concepts and ideas, from devices exploiting quantum interference [6–8] to schemes harnessing the valley degree of freedom [9]. In spite of the rapid progress, controlling or steering the flow of charge, spin, and valley currents across a device or material has remained a main challenge. A promising control path is achieving *one-way* transport, a situation where the current (of charge, valley, or spin) can flow among two electrodes in only one direction. An example is the recent realization of nonreciprocal supercurrent flow in a carbon nanotube [10]. An even more challenging path is seeking one-way transport in an isolator configuration. The isolator concept is borrowed from photonics [11] and is used here for a setup where transport is possible only from lead L to lead R but not in the opposite direction while the reflection at lead L vanishes [Fig. 1(a)]. As the scattering matrix associated with the two terminals in an isolator is nonunitary, achieving an isolator for electrons might seem impossible at first glance, but as will become clear later, this is not the case.

Here we show a proof of concept for an electronic isolator obtained by shining a laser on a bilayer graphene ribbon. A previous study [12] predicted a scheme for realizing this effect for charge (spin) transport on a biased bilayer graphene ribbon by including a Haldane (spin-orbit) term. In spite of the difficulty to realize a Haldane term [13] in condensed-matter experiments, our results show that laser illumination can take a similar role and be used to produce a targeted nonreciprocity. By offering a proof of concept, our work thus paves the way for new optoelectronic devices.

In the following we deepen the isolator concept and provide further motivation to this work before turning to our model and the results.

The isolator concept in optics. In optics, a device allowing light to pass in one direction but blocking it in the opposite one is called an *isolator* [11]. It is of great use in photonics where reflections that may, for example, reveal information to an observer intercepting the signal are undesired. Moreover, in an isolator, other effects such as spurious interferences and light rerouting can be lessened if not eliminated. An isolator requires at least two single-mode terminals connected to the device in such a way that transmission can occur from one terminal to the other but vanishes in the reciprocal direction. As noted in Ref. [11], the isolator has either to perfectly block the transmission in one direction or to divert it to a third terminal. Thus, the scattering matrix that represents an isolator must be asymmetric. For a two-terminal system with a single channel on each terminal an isolator and its corresponding scattering matrix would be as shown in Fig. 1(a).

Opportunities and challenges for the isolator concept in electronics. An isolatorlike effect is also desirable in other contexts, such as in electronics, where directional transport is useful for logical applications. Yet, to the best of our knowledge, the isolator is still missing from the tool kit of quantum devices. The first challenge is immediately apparent: in typical electronic devices the scattering matrix is warranted to be unitary, and as such, a skewed matrix like the one mentioned earlier is not possible. However, this is not an obstacle if we consider a system with a third electrode intended solely to reroute or divert the charges propagating in one direction. The effective scattering matrix for the two-terminal system may indeed be skewed in such a case without violating unitarity. But even when this issue can be circumvented by adding a third physical terminal, the challenge of how to get a perfectly nonreciprocal system, one where transmission from L to R is 1 and is 0 from R to L, remains.

If we think of systems hosting perfectly transmitting and robust states, the first one that comes to mind is a sample hosting chiral states like in the quantum Hall regime. But this also occurs in other nonequilibrium situations [14–16], such as in the case of graphene irradiated with a laser, where a gap opens (in both monolayer [14] and bilayer graphene [17–19]) and Floquet chiral edge states emerge in the spectrum [14,20–26]. Since the band structure in such systems is reciprocal, to get an isolatorlike behavior one would need to suppress transport through the states propagating along one of the edges. However, this is prevented by the

*vdallago@famaf.unc.edu.ar

†luis.foatorres@uchile.cl

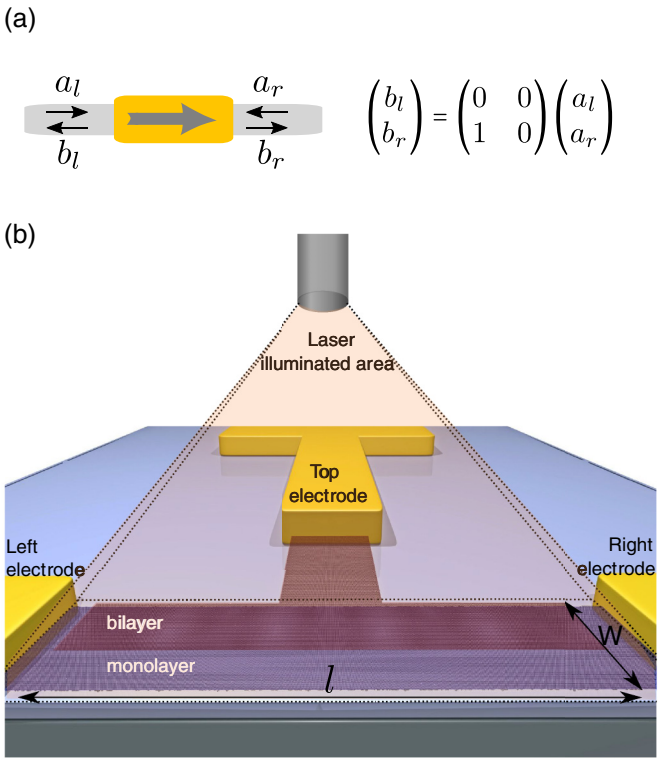

FIG. 1. (a) Scheme of the simplest ideal isolator (as discussed in Ref. [11]) where single-mode wires are connected to a sample. The scattering matrix is skewed, and transmission occurs only from left to right. (b) Scheme of the setup considered in this work to obtain an isolator effect: a laser-illuminated graphene sample connected to left and right electrodes, an inhomogeneous region with monolayer and bilayer graphene areas, and a third electrode on top. The bilayer area is biased perpendicularly to the graphene plane.

bulk-boundary correspondence, thereby requiring a scheme to circumvent it.

This work. Here we offer a proof of concept where an isolator effect is obtained in a laser-illuminated graphene bilayer ribbon. The proposed system has two "active" electrodes connected to one of the layers (which form the isolator) and a third electrode connected to the other layer which is used for diverting unwanted reflections [see scheme in Fig. 1(b)]. As will become clear later, since driving has a crucial role as it promotes the nonreciprocity in the electronic/valley transport, we call this device a *Floquet isolator*.

We should also comment on the difference from the large body of previous works aimed at obtaining directional charge transport using time-dependent fields. This includes, notably, the phenomenon called quantum pumping, the use of time-dependent potentials to steer transport and obtain a dc current at zero bias or even against an external bias voltage. In the open regime [27–29] quantum pumping usually relies on quantum interference and has been extensively studied for both the adiabatic [27,30–33] and nonadiabatic cases [29,34–37]. The proposal in this paper is different from those in several aspects. First, in our case the directionality is built into the electronic structure of the system, and second, the scattering matrix for a quantum pump does not generally have a perfect directionality as in an isolator.

Another related device, in which directional transport is obtained, is a diode. The isolator concept differs from the diode used in electronics in different ways: first, the isolator works even when the bias voltage between the source (L) and drain (R) is zero; second, unlike diodes, the direction of operation of the isolator can be reversed by changing an external control parameter. Furthermore, in a diode the mechanism underlying unidirectional transport is built on the generation of a depletion zone in a p-n junction.

Finally, there is also one interesting previous study [38] where optical nonreciprocity is produced through electrical driving. This is the converse of our proposal, where nonreciprocity in charge or valley transport is produced through laser illumination. There are also other recent works aimed at tailoring nonreciprocity but in interacting systems, like in Ref. [39], or by tuning individual matrix elements of the Hamiltonian by using time-dependent fields [40]. Another related proposal is that of Ref. [41] involving a ferromagnet on a topological insulator.

Nonreciprocity in transport means that the transmission probability, say from left to right, differs from that in the opposite direction, even if only by a tiny amount. In our case we use laser illumination to achieve a situation where transmission in one direction vanishes while in the opposite direction it takes a value close to unity as in an ideal isolator.

II. HAMILTONIAN MODEL AND FLOQUET SOLUTION SCHEME

To motivate our discussion we consider a simple Hamiltonian for the electronic excitations in bilayer graphene:

$$\mathcal{H} = \sum_i E_i\, c_i^\dagger c_i - \sum_{\langle i,j\rangle} \gamma_{i,j} c_i^\dagger c_j + \mathcal{H}_\perp, \tag{1}$$

where $c_i^\dagger$ and c_i are the electronic creation and annihilation operators at the π orbital on site i (which can be A type or B type, A_1 and B_1 for the lower layer and A_2 and B_2 for the upper one). The second summation runs over nearest neighbors, and the associated hopping matrix elements $\gamma_{i,j}$ are all taken equal to $\gamma_0 = 2.7$ eV [4], which is considered the unit of energy hereafter. All the dimensions are expressed in terms of the lattice constant $a = 0.246$ nm. To model a bias voltage applied perpendicularly to the graphene bilayer we include a shift of the site energies on the lower ($E_i = E_0 - \Delta/2$) and upper ($E_i = E_0 + \Delta/2$) layers. Without loss of generality we take $E_0 = 0$. We consider a bilayer graphene with Bernal stacking [see Fig. 2(c)]. In our model we consider the interlayer hopping matrix elements between the A_1 and B_2 sites, γ_1, which are included in $\mathcal{H}_\perp$ of the Hamiltonian.

It has been shown that laser-illuminated graphene monolayers [14,21,26,42] and bilayers [19,43,44] may host chiral edge states if the laser parameters are appropriately chosen [45]. These Floquet chiral edge states will be the "substrate" on which we will base our proposal.

Here we consider a sample irradiated with a circularly polarized laser perpendicular to the bilayer sample. This is incorporated in the Hamiltonian through the Peierls substitution as a time-dependent phase in the nearest-neighbor matrix

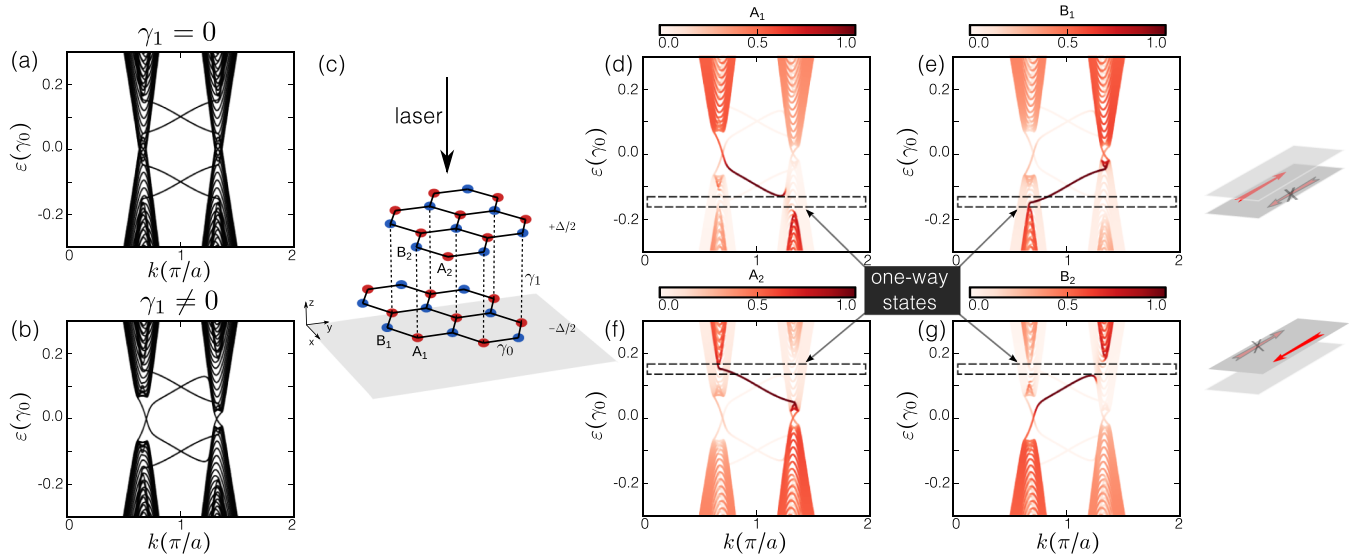

FIG. 2. (a) and (b) The full dispersion for the electronic states of a bilayer graphene ribbon with a bias voltage and irradiated with a laser, where the interlayer coupling is off and on, respectively. (c) Scheme of a graphene bilayer with Bernal stacking and a bias voltage applied perpendicularly. (d)–(g) The same dispersion as in (b) with a color scale encoding the weight of the states on sites A_1, B_1, A_2, and B_2 for the Floquet replica $n = 0$. The parameters are chosen with the aim of illustrating the proposed mechanism: $\Delta = 0.2$, $W = 103a$, $\hbar\Omega = 3.5$, and $z = 0.5$.

elements [46,47]:

$$\gamma_{ij}(t) = \gamma_0 \exp\left[i \frac{2\pi}{\Phi_0} \int_{\mathbf{r}_j}^{\mathbf{r}_i} \mathbf{A}(t) \cdot d\mathbf{r} \right], \tag{2}$$

where $\mathbf{A}(t)$ is the vector potential of the radiation and Φ_0 is the magnetic flux quantum. As can be seen, $\gamma(t)$ depends on the position of the two nearest-neighbor sites under consideration. Then, since the radiation is perpendicular to the graphene plane, there is no change in γ_1. Particularly, the vector potential associated with a circularly polarized monochromatic plane wave in the z direction (perpendicular to the graphene sheet) is $\mathbf{A}(t) = A_0[\sin(\Omega t)\,\hat{x} + \cos(\Omega t)\,\hat{y}]$, where Ω corresponds to the radiation frequency and A_0 determines the driving amplitude. The strength of the latter can also be characterized by the dimensionless parameter $z = A_0 a 2\pi/\Phi_0$.

The spectral and transport properties of this system can be calculated from the time-independent Floquet Hamiltonian ($\mathcal{H}_F = \mathcal{H} - i\hbar\partial_t$). This theory is a suitable approach due to the time periodicity ($2\pi/\Omega$ in our case) of the Hamiltonian. For a given $\mathcal{H}_F$ the eigenvalue problem, analogous to that of the time-independent Schrödinger equation, can be solved in the Floquet space. This space is defined as the direct product ($\mathscr{R} \otimes \mathscr{T}$) between the usual Hilbert space $\mathscr{R}$ and that of the time periodic functions $\mathscr{T}$ [48]. Particularly, there is a complete set of Floquet solutions of the form $\psi_\alpha(\boldsymbol{r},t) = \exp(-i\varepsilon_\alpha t/\hbar)\phi_\alpha(\boldsymbol{r},t)$, where ε_α are the so-called quasienergies and $\phi_\alpha(\boldsymbol{r},t+T) = \phi_\alpha(\boldsymbol{r},t)$ are the associated Floquet states. The $\mathscr{T}$ space is spanned by the $\exp(in\Omega t)$ functions, where the index n may be interpreted as the number of "photon" excitations and defines the nth Floquet replica subspace [49].

The calculations presented in the following sections were carried out with homemade codes built on the KWANT [50] module.

III. GENERATING A NONRECIPROCAL FLOQUET BAND STRUCTURE WITH UNBALANCED CHIRAL EDGE STATES

To design an isolator device we take advantage of the chiral edge states found in irradiated graphene samples [21,45,51] and look for a way of annihilating one of those. We aim to generate a nonreciprocal band structure, which means, generically, that $\varepsilon(k) \neq \varepsilon(-k)$. Here we are interested in the case where the chiral states are unbalanced (there is one edge state propagating in one direction and none in the opposite one) as this would improve our prospects for achieving unidirectional transport.

In Refs. [45,51], the authors have shown that when illuminating a graphene monolayer with a laser, a gap at zero energy opens in the dispersion relation (besides others at energies which are integer multiples of half the laser frequency), and chiral states propagating along the edges emerge. The width of the ribbons W simulated hereafter was chosen to have fully developed edge states on one of the layers. In this regime, the results are not sensitive to the particular value of W.

If we take the interlayer coupling of the bilayer graphene sample to be zero, then applying a perpendicular bias leads to a band structure that is equivalent to that of two laser-illuminated monolayers but shifted in energy [as shown in Fig. 2(a)]. Notably, on each monolayer one observes the opening of a gap around the Dirac point and edge states bridging them. When the interlayer coupling is turned on, one gets the results shown in Fig. 2(b). Besides the appearance of valley asymmetry due to the breaking of inversion symmetry, we see that the edge states bridging the laser-induced gap seem to remain almost intact.

A more compelling feature is hidden in this dispersion relation but can be revealed when coloring it according to the weight on the different sites of the bilayer. Figures 2(d)–2(g)

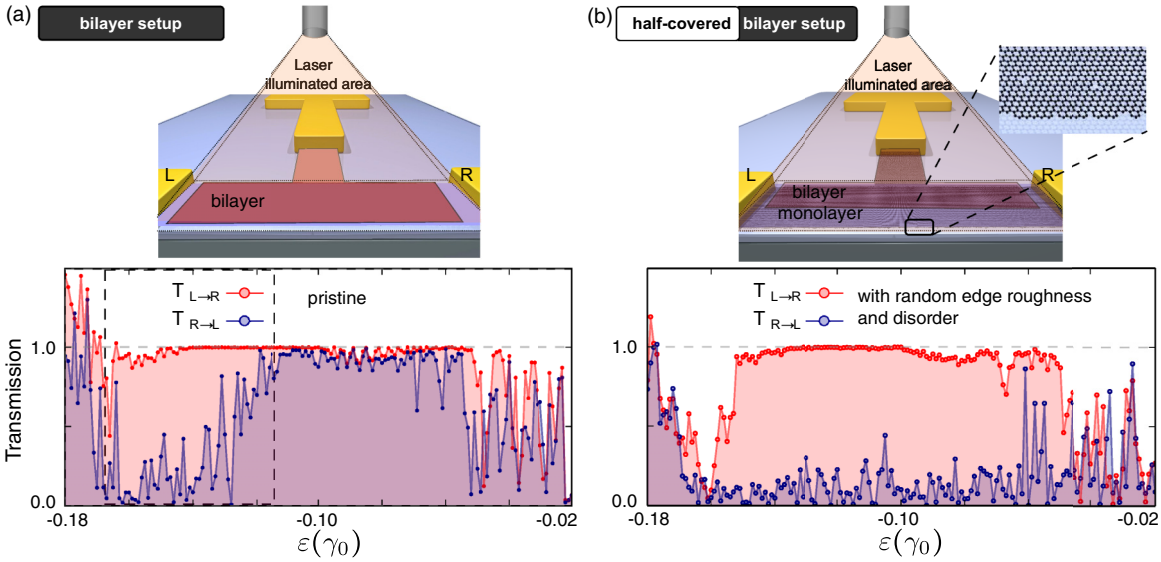

FIG. 3. (a) Top: Scheme of the three-terminal setup where a bilayer sample is connected to three monolayer graphene leads, two of them on the lower layer (L and R) and a third one on the upper layer. Bottom: Transmission probabilities between the left (L) and right (R) leads as a function of the electronic energy. One can see a strong directionality in the energy region marked with a dashed box in Figs. 2(d) and 2(g). (b) Same as (a) for the case where the upper layer covers only half of the lower one, with rough edges and 1 ‰ vacancies. In this setup directional transport is achieved throughout the full gap as explained in the text. The laser parameters are as in Fig. 2, $W = 103a$ and $l = 500a$.

present the spectrum with a color scale encoding the weight in the lower [Fig. 2(d) for site A_1 and Fig. 2(e) for B_1) and upper [sites A_2 in Fig. 2(f) and B_2 in Fig. 2(g)] layers. It can be noticed that the edge states in the bulk energy gap of each monolayer (centered at energy $\pm\Delta/2$) have a strong sublattice polarization (greater than 95%). The origin of this polarization is the radiation itself (which is responsible for the appearance of the chiral edge states), and it is also favored by the presence of the perpendicular bias.

However, the most significative characteristic exposed in Figs. 2(d) and 2(g) is the existence of a region of energy where the (weight of one) chiral edge state vanishes. This disappearance originates in the hybridization between the edge states in one layer and the continuum on the other one in the graphene sample. Specifically, due to the chosen Bernal stacking, sites A_1 interact with B_2 through γ_1 [shown in Fig. 2(c)]. Even though the value of γ_1 is small ($\gamma_1 = 0.1\gamma_0$), due to the high density of states in the metallic layer (at the energy of interest), it is enough to "switch off" the chiral edge state polarized in A_1 or B_2. On the other hand, the states polarized in A_2 or B_1 are more protected from the hybridization (due to the lack of a direct interaction) and so are more robust. As stated before, this annihilation of only one of the chiral edge states is our focus in order to build an isolator.

The radiation and the bias also have direct influence on where this effect is observed in the dispersion relation. In particular by changing the polarization the valley in which the hybridization occurs can be swapped.

IV. TRANSPORT PROPERTIES, ONE-WAY CHARGE TRANSPORT, AND THE ISOLATOR EFFECT

Illuminating the bilayer graphene sample with a circularly polarized laser breaks the time-reversal symmetry. The same result is attained for the inversion symmetry due to the external bias. Hence, the right-left symmetry in our system is broken. However, this cannot be exploited when connecting only two monolayer graphene leads to the sample. The unitarity of the 2×2 scattering matrix implies that the transmission from the left lead to the right one is equal to the transmission in the opposite direction. To elude this obstacle in the search of a *Floquet isolator*, a third monolayer graphene lead is incorporated by attaching it to the upper layer of the sample [see schemes in Figs. 3(a) and 3(b)]. The unitary is now compulsory for the new 3×3 scattering matrix, whereas the effective 2×2 one can be asymmetric, allowing us to profit from the nonreciprocity of the dispersion relation.

In Fig. 3(a) we show the left to right and right to left transmission probabilities for the irradiated bilayer graphene ribbon ($W = 103a$ and $l = 500a$). The chosen range of energy corresponds to the one at which one of the chiral edge states vanishes in the dispersion relation [Figs. 2(d) and 2(g)]. We assumed that the thermalization process occurs in the leads as usual in Floquet scattering theory [42,52]. Figure 3(a) shows how the nonreciprocity of the band structure is reflected as directional asymmetry in the transmissions.

Comparing our results to the ones of an ideal isolator (Fig. 1), we can notice that they differ in $T_{R\to L}$, which is not perfectly zero, although $T_{L\to R}$ is almost 1. Two main factors contribute to this small $T_{R\to L}$: (a) the unavoidable interface between illuminated and nonilluminated areas, which may lead to additional scattering (and which, indeed, produces a reflection filtering all but one transmission channel), and (b) the abrupt change from the bilayer sample to the graphene monolayer leads. Nonetheless, the directionality is still evident.

Ideally, an electronic isolator should be robust to disorder and roughness. This implies that its properties (like the directional asymmetry) will not be modified by details such

as the particular shape of the edges or the presence of edge roughness. However, the isolatorlike behavior presented up to now relies on the sublattice polarization of the Floquet chiral states [see Figs. 2(d)–2(g)], which allows for the upper layer to introduce a selective "environment" to the lower one thanks to the stacking order. Hence, the nonreciprocity might be jeopardized by a small distortion of the physical system (see Appendix A). In the following we present a different setup designed to circumvent this problem. As we will see, the new setup improves on all the mentioned weaknesses.

Let's now consider a monolayer graphene sample in which only one half is covered by a second layer, as shown in the scheme in Fig. 3(b). In this case the upper layer can be effective in hybridizing the edge states on only one side of the lower layer (the one in which it is present). In contrast, the states on the opposite edge remain decoupled from this particular environment. This improved setup takes advantage of both the robustness of the topological edge states of an irradiated graphene monolayer [20,21] and the nonreciprocal Floquet band structure of the laser-illuminated bilayer sample.

The new half-covered bilayer setup allows for transport to be resilient to edge roughness, stacking order, and disorder. We tested this idea by incorporating imperfections to the system. First, we added roughness to the terminations on both sides (originally of zigzag type). For each line of atoms perpendicular to the transport direction, we chose randomly a site within one lattice constant of the edge and made the lattice terminate at this site, removing the remaining dangling bonds. This resulted in a lattice with edge roughness as shown in the scheme in Fig. 3(b). Second, to further test the robustness of the transport response, we also added random vacancies to the upper layer of the sample. The vacancies are distributed randomly with a concentration of one vacancy per thousand atoms. Each vacancy is modeled by deleting the associated site from the original Hamiltonian.

The transmissions for the setup of the top panel of Fig. 3(b) with edge roughness and 1 ‰ vacancies are shown in the bottom panel of Fig. 3(b). It can be noticed that the directional asymmetry is preserved in this setup despite the presence of disorder and, even better, the asymmetry now extends over the full gap of the lower monolayer. Thus, directionality not only withstands imperfections but can even improve when they are added. This implies that the mechanism is *antifragile* [53] with respect to these parameters.

The antifragility of the sample is further illustrated in Fig. 4, where we show the transmission probabilities for a system analogous to the setup in Fig. 3(b) but with the opposite edge covered (the one terminated in B_1 sites). Figure 4(a) corresponds to the pristine case, whereas in Fig. 4(b) we show the transmission probabilities when including both edge roughness and disorder. The directionality is almost lost in the pristine system because the switch-off mechanism is ineffective when the covered edge state in the lower layer is polarized on the B_1 sublattice. However, when disorder is added, the directionality improves dramatically, and a result equivalent to the previous setup is obtained; that is, the directionality extends over the full gap of the monolayer.

One may wonder about the dependence of our results on the particular disorder realization and/or the laser parameters. Regarding the particular disorder or edge roughness

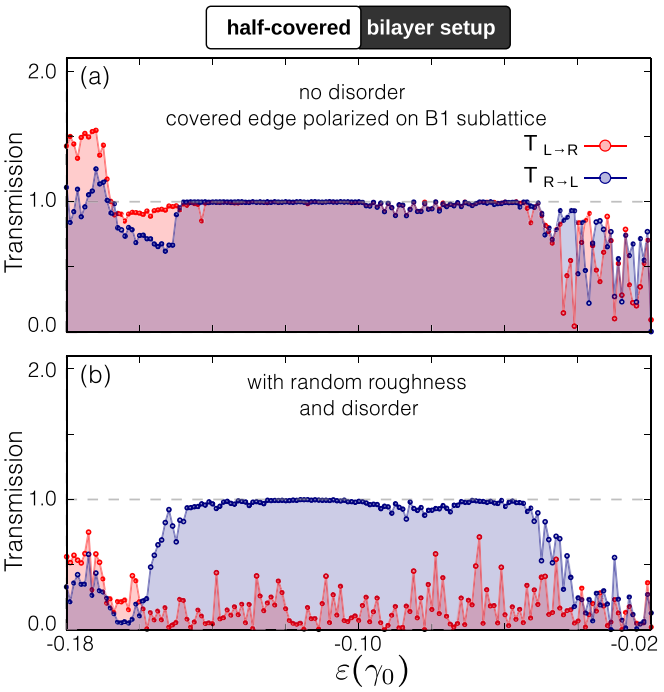

FIG. 4. Transmission probabilities as a function of the energy of the incoming electrons. Here the lower layer is half covered, and the corresponding zigzag edge state is polarized on the B_1 sublattice. The "switch-off" mechanism is ineffective, at least for the pristine system in (a) where the directionality is almost lost. The situation changes dramatically when edge roughness and disorder are added to the same sample, as shown in (b). The remaining system parameters are chosen as in Fig. 3(b).

configuration, we find that the results remain qualitatively the same with only small changes (see Appendix A). As for the laser parameters, the laser frequency and intensity control the magnitude of the gap in the time-averaged density of states, thereby setting the energy range in which the directionality is seen, the size of the currents, and the experimental feasibility of the setup. In Appendix B we show the transmission probabilities for two additional values of the laser intensity, in which it can be noticed that the results remain qualitatively the same.

The frequency and intensity of the laser employed here were chosen in order to make the numerics less demanding. However, using the known scaling of the laser-induced gaps with the laser parameters [14,54], one can estimate the most suitable laser frequency for experimental observation, which turns out to be the midinfrared [54] (as used in the experiments of Ref. [55]). This is certainly not quite practical but serves the purpose of a proof-of-principle setup. The obtained time-averaged currents have a magnitude of $(2e/h)\Delta$, where $\Delta \simeq 2(eA_0v_F)^2\hbar\Omega$ is the magnitude of the gap in the time-averaged density of states of the lower monolayer at the Dirac point (with v_F being the Fermi velocity). As pointed out in Ref. [54], for a laser frequency in the midinfrared with $\hbar\Omega = 140$ meV, a laser power of 130 mW/μm^2 would result in a laser-induced gap at the Dirac point of about 30 meV and currents of about 2μA.

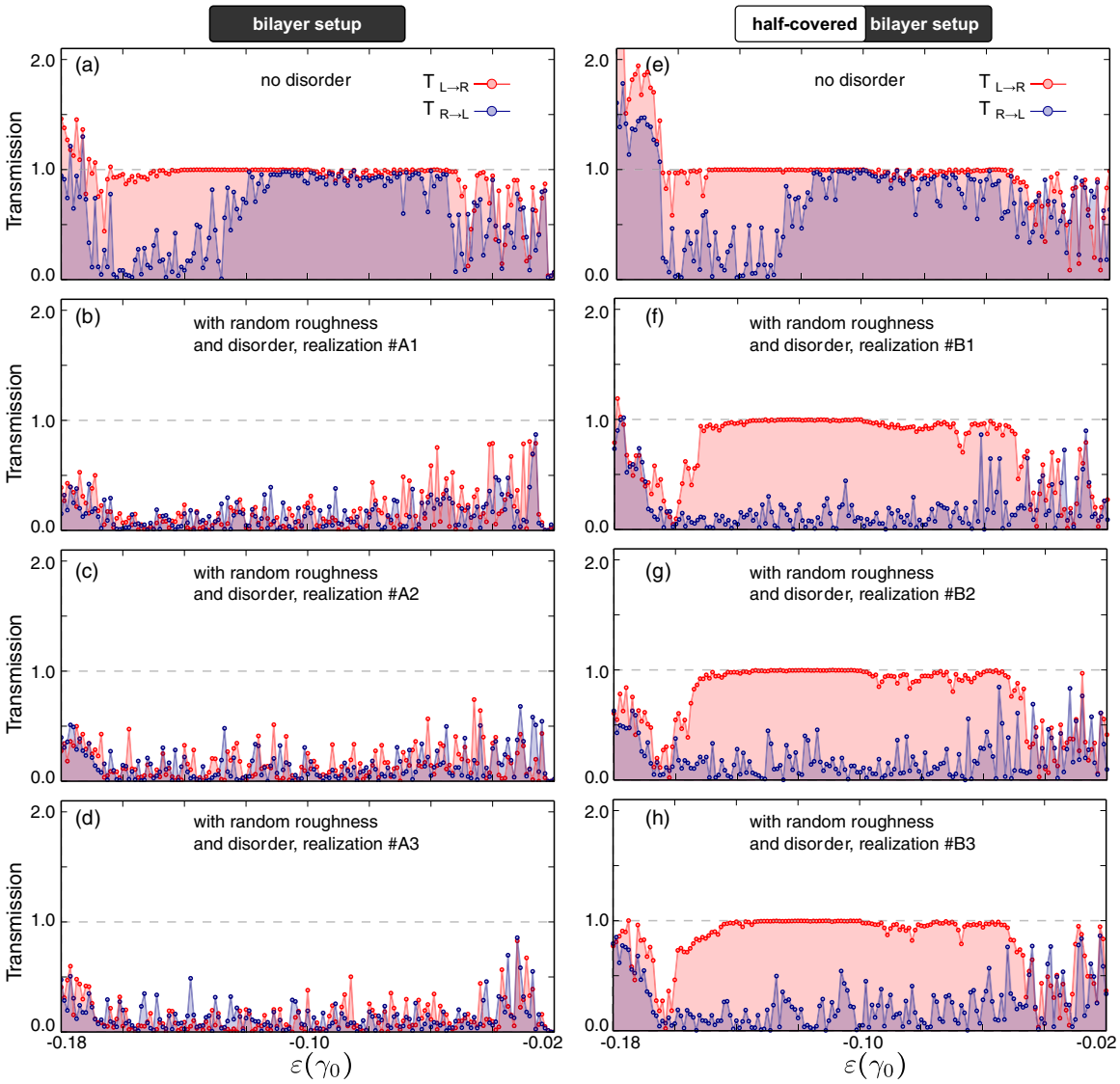

FIG. 5. Numerical results for the transmission probabilities of the setups considered in the text for (a)–(d) the bilayer setup and (e)–(h) the half-covered bilayer setup. The results correspond to pristine systems [(a) and (e)] and samples with different realizations of disorder and edge roughness. The parameters are the same as in Fig. 3.

V. SUMMARY AND FINAL REMARKS

Isolators, devices where transmission occurs in one direction and is suppressed in the opposite one, have been missing from the tool kit of available devices in electronics. Here we presented a demonstration of this effect for the case of a laser-illuminated graphene bilayer ribbon. Laser illumination allows us to introduce an effective Haldane-like term [13] which together with the inversion symmetry breaking (produced by an electric field perpendicular to the graphene bilayer) allows for a nonreciprocal band structure, which is exploited to produce an isolator effect.

Our starting point in this paper is the Floquet topological states produced by laser illumination on graphene. By covering a single edge of the system [as in Fig. 1(b)] we showed how a selective *switching off* of the sites at one of the edges can be achieved. This directionality is then exploited to produce one-way transport. Interestingly, the directionality improves with edge roughness and disorder; it is antifragile [53] with respect to those parameters. This implies that, rather than being merely resilient to disorder, the effect actually improves or gets better with it.

By offering a proof of concept, our work thus paves the way for new optoelectronic devices exploiting the one-way characteristic of the topological states for more efficient transport of energy, charge, or spin. We hope that these results will stimulate the search for new ways of tailoring and harnessing nonreciprocity in electronic systems both theoretically and experimentally.

ACKNOWLEDGMENTS

V.D.L. acknowledges funding from CONICET. L.E.F.F.T. acknowledges funding by Program “Inserción Académica”

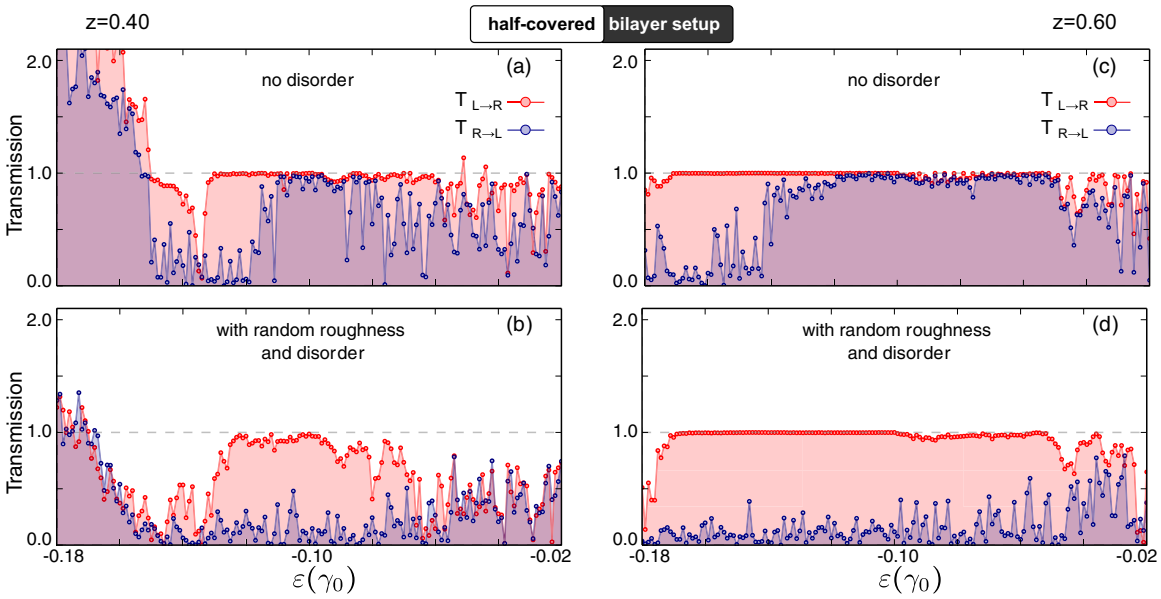

FIG. 6. Transmission probabilities for the half-covered bilayer setup [(b) and (d)] with and [(a) and (c)] without disorder and edge roughness for two different values of the laser intensity given by the dimensionless parameter z. The remaining system parameters are chosen as in Fig. 3(b).

2016 of the University of Chile and FondeCyT Regular No. 1170917 (Chile).

L.E.F.F.T., V.D.L., and E.S.M. developed the concept. L.E.F.F.T. and V.D.L. designed the study. V.D.L. wrote a code and obtained the numerical results shown here; L.E.F.F.T. verified the main results. V.D.L. and L.E.F.F.T. wrote the manuscript and prepared the figures. The text was discussed and agreed on by all the authors.

APPENDIX A: ADDITIONAL RESULTS FOR THE CALCULATIONS WITH DISORDER AND EDGE ROUGHNESS

Figure 5 shows the numerical results for the transmission probabilities of both setups considered in the text [bilayer setup in Figs. 5(a)–5(d) and half-covered bilayer setup in Figs. 5(e)–5(h)]. Figures 5(a) and 5(e) are for pristine samples, and the other plots correspond to different realizations of disorder and edge roughness in the ribbons. The parameters are the same as in Fig. 3. Different disorder/edge roughness realizations do not show important variations. While in the bilayer setup the transport directionality is jeopardized when adding disorder and edge roughness, in the half-covered bilayer setup it improves.

APPENDIX B: ADDITIONAL RESULTS FOR THE ROLE OF THE LASER PARAMETERS

Figure 6 shows the transmission probabilities for the half-covered bilayer setup with and without disorder and edge roughness for two different values of the laser intensity. Despite the differences, the results remain qualitatively the same as those shown and explained in the main text.

[1] K. S. Novoselov, A. K. Geim, S. V. Morozov, D. Jiang, Y. Zhang, S. V. Dubonos, I. V. Grigorieva, and A. A. Firsov, Electric field effect in atomically thin carbon films, Science **306**, 666 (2004).

[2] K. S. Novoselov, A. K. Geim, S. V. Morozov, D. Jiang, M. I. Katsnelson, I. V. Grigorieva, S. V. Dubonos, and A. A. Firsov, Two-dimensional gas of massless Dirac fermions in graphene, Nature (London) **438**, 197 (2005).

[3] Y. Zhang, Y.-W. Tan, H. L. Stormer, and P. Kim, Experimental observation of the quantum Hall effect and Berry's phase in graphene, Nature (London) **438**, 201 (2005).

[4] A. H. Castro Neto, F. Guinea, N. M. R. Peres, K. S. Novoselov, and A. K. Geim, The electronic properties of graphene, Rev. Mod. Phys. **81**, 109 (2009).

[5] A. K. Geim and I. V. Grigorieva, Van der Waals heterostructures, Nature (London) **499**, 419 (2013).

[6] P. Rickhaus, R. Maurand, M.-H. Liu, M. Weiss, K. Richter, and C. Schönenberger, Ballistic interferences in suspended graphene, Nat. Commun. **4**, 2342 (2013).

[7] A. L. Grushina, D.-K. Ki, and A. F. Morpurgo, A ballistic pn junction in suspended graphene with split bottom gates, Appl. Phys. Lett. **102**, 223102 (2013).

[8] P. Gehring, H. Sadeghi, S. Sangtarash, C. S. Lau, J. Liu, A. Ardavan, J. H. Warner, C. J. Lambert, G. A. D. Briggs, and J. A. Mol, Quantum interference in graphene nanoconstrictions, Nano Lett. **16**, 4210 (2016).

[9] J. R. Schaibley, H. Yu, G. Clark, P. Rivera, J. S. Ross, K. L. Seyler, W. Yao, and X. Xu, Valleytronics in 2D materials, Nat. Rev. Mater. **1**, 16055 (2016).

[10] F. Qin, W. Shi, T. Ideue, M. Yoshida, A. Zak, R. Tenne, T. Kikitsu, D. Inoue, D. Hashizume, and Y. Iwasa, Superconductivity in a chiral nanotube, Nat. Commun. **8**, 14465 (2017).

[11] D. Jalas, A. Petrov, M. Eich, W. Freude, S. Fan, Z. Yu, R. Baets, M. Popovic, A. Melloni, J. D. Joannopoulos, M. Vanwolleghem, C. R. Doerr, and H. Renner, What is—and what is not—an optical isolator, Nat. Photonics **7**, 579 (2013).
[12] L. E. F. Foa Torres, V. Dal Lago, and E. S. Morell, Crafting zero-bias one-way transport of charge and spin, Phys. Rev. B **93**, 075438 (2016).
[13] F. D. M. Haldane, Model for a Quantum Hall Effect without Landau Levels: Condensed-Matter Realization of the "Parity Anomaly," Phys. Rev. Lett. **61**, 2015 (1988).
[14] T. Oka and H. Aoki, Photovoltaic Hall effect in graphene, Phys. Rev. B **79**, 081406 (2009).
[15] N. H. Lindner, G. Refael, and V. Galitski, Floquet topological insulator in semiconductor quantum wells, Nat. Phys. **7**, 490 (2011).
[16] J. Cayssol, B. Dóra, F. Simon, and R. Moessner, Floquet topological insulators, Phys. Status Solidi RRL **7**, 101 (2013).
[17] D. S. L. Abergel and T. Chakraborty, Generation of valley polarized current in bilayer graphene, Appl. Phys. Lett. **95**, 062107 (2009).
[18] D. S. L. Abergel and T. Chakraborty, Irradiated bilayer graphene, Nanotechnology **22**, 015203 (2011).
[19] E. S. Morell and L. E. F. Foa Torres, Radiation effects on the electric properties of bilayer graphene, Phys. Rev. B **86**, 125449 (2012).
[20] T. Kitagawa, T. Oka, A. Brataas, L. Fu, and E. Demler, Transport properties of nonequilibrium systems under the application of light: Photoinduced quantum Hall insulators without Landau levels, Phys. Rev. B **84**, 235108 (2011).
[21] P. M. Perez-Piskunow, G. Usaj, C. A. Balseiro, and L. E. F. Foa Torres, Floquet chiral edge states in graphene, Phys. Rev. B **89**, 121401(R) (2014).
[22] A. Kundu, H. A. Fertig, and B. Seradjeh, Effective Theory of Floquet Topological Transitions, Phys. Rev. Lett. **113**, 236803 (2014).
[23] H. Dehghani, T. Oka, and A. Mitra, Dissipative Floquet topological systems, Phys. Rev. B **90**, 195429 (2014).
[24] A. Gómez-León, P. Delplace, and G. Platero, Engineering anomalous quantum Hall plateaus and antichiral states with ac fields, Phys. Rev. B **89**, 205408 (2014).
[25] A. López, A. Scholz, B. Santos, and J. Schliemann, Photoinduced pseudospin effects in silicene beyond the off-resonant condition, Phys. Rev. B **91**, 125105 (2015).
[26] L. Du, X. Zhou, and G. A. Fiete, Quadratic band touching points and flat bands in two-dimensional topological Floquet systems, Phys. Rev. B **95**, 035136 (2017).
[27] P. W. Brouwer, Scattering approach to parametric pumping, Phys. Rev. B **58**, R10135 (1998).
[28] B. L. Altshuler and L. I. Glazman, Pumping electrons, Science **283**, 1864 (1999).
[29] B. Kaestner and V. Kashcheyevs, Non-adiabatic quantized charge pumping with tunable-barrier quantum dots: A review of current progress, Rep. Prog. Phys. **78**, 103901 (2015).
[30] E. Prada, P. San-Jose, and H. Schomerus, Quantum pumping in graphene, Phys. Rev. B **80**, 245414 (2009).
[31] R. Zhu and H. Chen, Quantum pumping with adiabatically modulated barriers in graphene, Appl. Phys. Lett. **95**, 122111 (2009).
[32] L. H. Ingaramo and L. E. F. Foa Torres, Quantum charge pumping in graphene-based devices: When lattice defects do help, Appl. Phys. Lett. **103**, 123508 (2013).
[33] H. Khani, M. Esmaeilzadeh, and F. Kanjouri, Controllable quantum valley pumping with high current in a silicene junction, Nanotechnology **27**, 495202 (2016).
[34] L. Arrachea, Green-function approach to transport phenomena in quantum pumps, Phys. Rev. B **72**, 125349 (2005).
[35] L. E. F. Foa Torres, Mono-parametric quantum charge pumping: Interplay between spatial interference and photon-assisted tunneling, Phys. Rev. B **72**, 245339 (2005).
[36] L. E. F. Foa Torres, H. L. Calvo, C. G. Rocha, and G. Cuniberti, Enhancing Single-Parameter Quantum Charge Pumping in Carbon-Based Devices, Appl. Phys. Lett. **99**, 092102 (2011).
[37] A. Croy, U. Saalmann, A. R. Hernández, and C. H. Lewenkopf, Nonadiabatic electron pumping through interacting quantum dots, Phys. Rev. B **85**, 035309 (2012).
[38] H. Lira, Z. Yu, S. Fan, and M. Lipson, Electrically Driven Nonreciprocity Induced by Interband Photonic Transition on a Silicon Chip, Phys. Rev. Lett. **109**, 033901 (2012).
[39] T. Morimoto and N. Nagaosa, Nonreciprocal current of strongly correlated electrons in noncentrosymmetric crystals, arXiv:1706.08991.
[40] H. Li, T. Kottos, and B. Shapiro, Non-reciprocal transport due to losses and Floquet engineered directed bonds, arXiv:1710.05399.
[41] F. Mahfouzi, B. K. Nikolić, S.-H. Chen, and C.-R. Chang, Microwave-driven ferromagnet–topological-insulator heterostructures: The prospect for giant spin battery effect and quantized charge pump devices, Phys. Rev. B **82**, 195440 (2010).
[42] Z. Gu, H. A. Fertig, D. P. Arovas, and A. Auerbach, Floquet Spectrum and Transport Through an Irradiated Graphene Ribbon, Phys. Rev. Lett. **107**, 216601 (2011).
[43] C. Qu, C. Zhang, and F. Zhang, Valley-selective topological ordered states in irradiated bilayer graphene, 2D Mater. **5**, 011005 (2018).
[44] I. V. Iorsh, K. Dini, O. V. Kibis, and I. A. Shelykh, Optically induced Lifshitz transition in bilayer graphene, Phys. Rev. B **96**, 155432 (2017).
[45] P. M. Perez-Piskunow, L. E. F. Foa Torres, and G. Usaj, Hierarchy of Floquet gaps and edge states for driven honeycomb lattices, Phys. Rev. A **91**, 043625 (2015).
[46] H. L. Calvo, P. M. Perez-Piskunow, H. M. Pastawski, S. Roche, and L. E. F. Foa Torres, Non-perturbative effects of laser illumination on the electrical properties of graphene nanoribbons, J. Phys. Condens. Matter **25**, 144202 (2013).
[47] H. L. Calvo, P. M. Perez-Piskunow, S. Roche, and L. E. F. Foa Torres, Laser-induced effects on the electronic features of graphene nanoribbons, Appl. Phys. Lett. **101**, 253506 (2012).
[48] H. Sambe, Steady states and quasienergies of a quantum-mechanical system in an oscillating field, Phys. Rev. A **7**, 2203 (1973).
[49] J. H. Shirley, Solution of the Schrödinger equation with a Hamiltonian periodic in time, Phys. Rev. **138**, B979 (1965).
[50] C. W. Groth, M. Wimmer, A. R. Akhmerov, and X. Waintal, Kwant: A software package for quantum transport, New J. Phys. **16**, 063065 (2014).
[51] G. Usaj, P. M. Perez-Piskunow, L. E. F. Foa Torres, and C. A. Balseiro, Irradiated graphene as a tunable Floquet topological insulator, Phys. Rev. B **90**, 115423 (2014).

[52] L. E. F. Foa Torres, P. M. Perez-Piskunow, C. A. Balseiro, and G. Usaj, Multiterminal Conductance of a Floquet Topological Insulator, Phys. Rev. Lett. **113**, 266801 (2014).

[53] N. N. Taleb, *Antifragile: Things That Gain from Disorder* (Random House, New York, 2012).

[54] H. L. Calvo, H. M. Pastawski, S. Roche, and L. E. F. Foa Torres, Tuning laser-induced band gaps in graphene, Appl. Phys. Lett. **98**, 232103 (2011).

[55] Y. H. Wang, H. Steinberg, P. Jarillo-Herrero, and N. Gedik, Observation of Floquet-Bloch states on the surface of a topological insulator, Science **342**, 453 (2013).